Hepatocyte-specific Pten deficiency results in steatohepatitis and hepatocellular carcinomas

Yasuo Horie,[1] Akira Suzuki,[2] Ei Kataoka,[1] Takehiko Sasaki,[3,4] Koichi Hamada,[2] Junko Sasaki,[2] Katsunori Mizuno,[3] Go Hasegawa,[5] Hiroyuki Kishimoto,[2] Masahiro Iizuka,[1] Makoto Naito,[5] Katsuhiko Enomoto,[6] Sumio Watanabe,[1] Tak Wah Mak,[7] and Toru Nakano[8]

[1]Department of Gastroenterology, [2]Department of Molecular Biology, and [3]21st Century COE Program, Akita University School of Medicine, Akita, Japan. [4]Precursory Research for Embryonic Science and Technology (PRESTO), Japan Science and Technology Agency (JST), Kawaguchi, Saitama, Japan. [5]Department of Cellular Function, Niigata University Graduate School of Medical and Dental Sciences, Niigata, Japan. [6]Department of Pathology, Akita University School of Medicine, Akita, Japan. [7]Advanced Medical Discovery Institute and Departments of Immunology and Medical Biophysics, University of Toronto, Toronto, Ontario, Canada. [8]Department of Pathology, Medical School and Graduate School of Frontier Biosciences, Osaka University, Osaka, Japan.

***PTEN* is a tumor suppressor gene mutated in many human cancers, and its expression is reduced or absent in almost half of hepatoma patients. We used the Cre-*loxP* system to generate a hepatocyte-specific null mutation of *Pten* in mice (*AlbCrePten*$^{flox/flox}$ mice). *AlbCrePten*$^{flox/flox}$ mice showed massive hepatomegaly and steatohepatitis with triglyceride accumulation, a phenotype similar to human nonalcoholic steatohepatitis. Adipocyte-specific genes were induced in mutant hepatocytes, implying adipogenic-like transformation of these cells. Genes involved in lipogenesis and β-oxidation were also induced, possibly as a result of elevated levels of the transactivating factors PPARγ and SREBP1c. Importantly, the loss of Pten function in the liver led to tumorigenesis, with 47% of *AlbCrePten*$^{flox/flox}$ livers developing liver cell adenomas by 44 weeks of age. By 74–78 weeks of age, 100% of *AlbCrePten*$^{flox/flox}$ livers showed adenomas and 66% had hepatocellular carcinomas. *AlbCrePten*$^{flox/flox}$ mice also showed insulin hypersensitivity. In vitro, *AlbCrePten*$^{flox/flox}$ hepatocytes were hyperproliferative and showed increased hyperoxidation with abnormal activation of protein kinase B and MAPK. Pten is thus an important regulator of lipogenesis, glucose metabolism, hepatocyte homeostasis, and tumorigenesis in the liver.**

Introduction

PTEN is a ubiquitously expressed tumor suppressor gene (1) that is mutated in many human sporadic cancers as well as in tumorigenic hereditary disorders such as Cowden disease. PTEN is a multifunctional phosphatase whose lipid phosphatase activity is associated with tumor suppression (2). The major substrate of PTEN is phosphatidylinositol-3,4,5-triphosphate (PIP3) (3), a lipid second-messenger molecule generated by the action of PI3Ks. PI3Ks are activated by a range of stimuli, including various cytokines and insulin. PIP3 activates the serine-threonine kinase protein kinase B (PKB/Akt), which is involved in antiapoptosis, proliferation, and oncogenesis.

While mutation of *PTEN* is an infrequent event in hepatocytes (4), PTEN protein expression is decreased or absent in about half of primary hepatoma patients (5). Decreased PTEN expression correlates with increased tumor grade, advanced disease stage, and poor prognosis (5). In vitro, administration of hepatocyte growth factor induces cellular proliferation via activation of the PI3K pathway (6), and hepatocyte cell lines that activate PKB/Akt resist apoptosis (7). These findings suggest that PTEN is important for maintaining homeostasis and preventing oncogenesis in the liver.

Nonstandard abbreviations used: acetyl-CoA carboxylase (ACC); acyl-CoA oxidase (AOX); alanine aminotransferase (ALT); alkaline phosphatase (ALP); aspartate aminotransferase (AST); 3,3′-diaminobenzidine (DAB); extracellular signal-regulated kinase (ERK); fatty acid synthetase (FAS); forkhead box transcription factor class O-1 (Foxo1); hepatocellular carcinoma (HCC); insulin receptor substrate (IRS); nonalcoholic steatohepatitis (NASH); peroxisomal enoyl-CoA hydratase/3-hydroxyacyl-CoA dehydrogenase bifunctional protein (L-PBE); peroxisomal 3-ketoacyl-CoA thiolase (PTL); phosphatase and tensin homolog deleted from chromosome 10 (Pten); phosphatidylinositol-3,4,5-trisphosphate (PIP3); protein kinase B (PKB/Akt); reactive oxygen species (ROS); steroyl-CoA desaturase 1 (SCD1).

Conflict of interest: The authors have declared that no conflict of interest exists.

Citation for this article: *J. Clin. Invest.* **113**:1774–1783 (2004). doi:10.1172/JCI200420513.

The PPARs belong to the nuclear receptor superfamily (8). The PPAR subfamily comprises three isotypes: PPARα, PPARγ, and PPARβ/δ. These proteins all possess a highly conserved DNA-binding domain that recognizes peroxisome proliferator response elements in the promoter regions of target genes involved in lipid homeostasis (9). In particular, PPARγ is a key regulator of adipogenesis (9). Forced expression of PPARγ initiates the differentiation of fibroblasts into adipocytes via the induction of adipocyte-specific genes, leading to lipid accumulation (8). Similarly, forced expression of PPARγ in the liver triggers adipocyte-specific gene expression and steatosis (hepatic lipid accumulation) (10). The related receptor PPARα regulates enzymes involved in the β-oxidation of fatty acids, and is essential for the pleiotropic responses induced in the liver by peroxisome proliferators (11). Forced expression of PPARγ upregulates enzymes involved in PPARα-regulated peroxisomal fatty acid β-oxidation, including acyl-CoA oxidase (AOX), peroxisomal enoyl-CoA hydratase/3-hydroxyacyl-CoA dehydrogenase bifunctional protein (L-PBE), and peroxisomal 3-ketoacyl-CoA thiolase (PTL) (10, 12).

We have previously generated null *Pten*$^{-/-}$ mice as well as mice bearing tissue-specific Pten mutations in T, B, neuronal, cardiac muscle, and germ cells, as well as keratinocytes (all reviewed in ref. 13). In this study, we demonstrate that hepatocyte-specific Pten deficiency leads to steatohepatitis associated with increased PPARγ expression, insulin hypersensitivity, and liver tumorigenesis. PTEN is thus important for the maintenance of normal hepatocyte glucose metabolism as well as the prevention of adipogenic or tumorigenic transformation.

Methods

Generation of AlbCrePten$^{flox/flox}$ *mice.* *Pten*$^{flox/flox}$ mice (129Ola × C57BL6/J F_2), generated as previously described (14), were mated to *AlbCre* transgenic mice (C57BL6/J background; The Jackson

Laboratory, Bar Harbor, Maine, USA) (15), in which expression of Cre is controlled by the promoter of the hepatocyte-specific gene *Albumin*. Offspring carrying *AlbCre* and two copies of the floxed *Pten* allele (*AlbCrePten*$^{flox/flox}$), *AlbCre* plus one copy of the floxed *Pten* allele (*AlbCrePten*$^{flox/+}$), and *AlbCre* plus two copies of the WT *Pten* allele (*AlbCrePten*$^{+/+}$) were used in the analyses as homozygous mutant (*AlbCrePten*$^{flox/flox}$), heterozygous mutant (*AlbCrePten*$^{flox/+}$), and WT (*AlbCrePten*$^{+/+}$) mice, respectively.

Mice of 40 weeks of age that were part of the tumor burden experiments were excluded from all histological and biochemical assays except those described in Results under the heading *Tumor formation in the livers of AlbCrePten*$^{flox/flox}$ *mice*. All animal experiments were approved by the Institutional Review Board of the Akita University School of Medicine.

PCR analysis of Pten genotypes. Genomic DNA from mouse tails was isolated and amplified by PCR as described (16). Sequences of sense and antisense primers for the floxed and WT *Pten* alleles and the *AlbCre* transgene are given in Supplemental Table 1 (supplemental material available at http://www.jci.org/cgi/content/full/113/12/1774/DC1). Amplified fragments of 512 bp (floxed *Pten*), 413 bp (WT *Pten*), and about 550 bp (*AlbCre* transgene) were obtained.

Determination of total liver cell numbers. Livers were perfused in situ with oxygenated 0.5 mM EGTA containing calcium-free salt solution (10 ml/min at 37°C for 5 minutes), followed by perfusion with 0.04% collagenase type I (Wako Pure Chemicals Industries, Osaka, Japan) for 10 minutes as previously described (17). Livers were minced in a petri dish, filtered using Cell Strainer (Becton Dickinson Labware, Bedford, Massachusetts, USA), and repeatedly washed with PBS. Residual liver cells were collected in the same tube by pressing through the Cell Strainer using a syringe, and the total cell number was determined by Giemsa nuclear staining.

Southern and Western blots. Genomic Southern blots of total liver cell DNA were performed as described (16). For PKB/Akt, forkhead box transcription factor class O-1 (Foxo1, also known as FKHR), and MAPK assays, 100 μg of total liver cell lysate were analyzed by Western blotting as described (18). Antibody specific to the N terminus of Pten and to actin were from Santa Cruz Biotechnology (Santa Cruz, California, USA), while antibodies specific to phospho-PKB/Akt (Ser473), to total PKB/Akt, to phospho-MAPK (p42/p44; Thr202/Tyr204), to total MAPK (p42/p44), to phospho-Foxo1 (FKHR; Ser256), and to total Foxo1 were from New England Biolabs Inc. (Beverly, Massachusetts, USA).

Histology and immunohistology. Formalin-fixed tissues were embedded in paraffin using standard procedures. Sections (4 μm thick) were cut and stained with either H&E for standard microscopy or Azan stain to show fibrosis. To visualize lipids, frozen sections (5 μm thick) were stained with Oil Red O (Nakarai Tesque Inc., Kyoto, Japan) and counterstained with hematoxylin. For immunohistochemistry, sections from frozen tissues were fixed in 4% paraformaldehyde in PBS, blocked with 5% normal donkey serum (Chemicon International, Temecula, California, USA) plus 3% BSA, and incubated overnight with rabbit anti-mouse adiponectin antibody (provided by P.E. Scherer, Albert Einstein College of Medicine, New York, New York, USA) followed by Cy3-conjugated AffiniPure donkey anti-rabbit IgG (H+L) (The Jackson Laboratory) as a secondary antibody. To reveal adiponectin/albumin co-staining, the same sections were also incubated with rabbit anti-mouse albumin antibody (Biogenesis Ltd., Poole, United Kingdom) labeled with Alexa Fluor 488 using a rabbit IgG labeling kit (Molecular Probes Inc., Eugene, Oregon, USA). Double-stained sections were analyzed using confocal fluorescent microscopy (Leica Microsystems Inc., Deerfield, Illinois, USA). Peroxisomes in livers were detected by staining for catalase. Frozen liver sections (9 μm thick) were incubated overnight at 37°C with 5 mM 3,3′-diaminobenzidine (DAB) substrate in 0.1 M glycine-NaOH (pH 10.5)–0.15% H_2O_2. Nuclear counterstaining was performed with hematoxylin.

Electron microscopy. Mouse livers were perfused with 1.6% glutaraldehyde (TAAB Laboratory Equipment Ltd., Reading, United Kingdom), excised, and fixed at 4°C for 1 hour prior to examination using standard electron-microscopic techniques.

Lipid analysis. Mice were starved for a minimum of 8 hours and sacrificed by CO_2 asphyxiation. Blood was collected aseptically by cardiac puncture and centrifuged (13,000 *g*, 5 minutes, 4°C) to collect plasma. Total lipids were extracted from the liver as previously described (19). Levels of free cholesterol, cholesterol esters, FFAs, phospholipids and triglycerides in the liver, and total cholesterol, triglycerides, aspartate aminotransferase (AST), alanine aminotransferase (ALT), and alkaline phosphatase (ALP) in serum were determined by colorimetric, UV kinetic, or enzymatic assays following the various manufacturers' protocols (Sigma-Aldrich, St. Louis, Missouri, USA, and Wako Pure Chemicals Industries).

The fatty acid composition of the hepatic lipid fraction was analyzed by gas chromatography (20). After methanolysis by a modified Morrison and Smith method in which boron trifluoride served as the catalyst (20, 21), fatty acid methyl esters were analyzed using a Shimadzu GC-7A gas chromatograph (Shimadzu Corp., Kyoto, Japan) equipped with a capillary column of 30 m length × 0.3 mm diameter, coated with ethylene glycol succinate. The concentration of each fatty acid and the total amount of each fatty acid per liver were calculated as described previously (22).

RT-PCR. Total RNA was extracted using TRIzol (Life Technologies Inc., Gaithersburg, Maryland, USA) according to the manufacturer's instructions. Total RNA (1 μg) was reverse-transcribed using MMTV reverse transcriptase and the PCR protocol recommended by the manufacturer (Life Technologies Inc.). Primers for PCR reactions and numbers of PCR cycles are given in Supplemental Table 1. Amplified product sizes were as follows: PPARγ, 506 bp; PPARα, 463 bp; SREBP1c, 116 bp; C/EBPα, 411 bp; C/EBPβ, 195 bp; C/EBPδ, 280 bp; adiponectin, 132 bp; adipsin, 265 bp; aP2, 83 bp; fatty acid synthetase (FAS), 327 bp; acetyl-CoA carboxylase (ACC), 729 bp; stearoyl-CoA desaturase (SCD1), 271 bp; AOX, 536 bp; L-PBE, 356 bp; PTL, 293 bp; β-actin, 663 bp. The intensity of each band was measured using NIH image software.

BrdU staining. Mice were fed BrdU (3 mg/ml, Sigma-Aldrich) dissolved in drinking water for 4 days and sacrificed. Tissues were fixed in 10% neutral-buffered formalin and embedded in paraffin. Sections (4 μm thick) were deparaffinized and treated with HCl (2 N) for 20 minutes followed by 0.1% trypsin type II (crude from porcine pancreas; Sigma-Aldrich) for 20 minutes. Treated sections were incubated with normal goat serum (DAKO A/S, Glostrup, Denmark) for 1 hour, then with mouse anti-BrdU antibody (Becton Dickinson and Co., Franklin Lakes, New Jersey, USA) for 1 hour. Peroxidase-conjugated goat anti-mouse IgG (DAKO A/S) and DAB were used to detect BrdU incorporation. Normal mouse serum was used as the negative control. Slides were counterstained with hematoxylin.

TUNEL assay. Apoptosis was determined by the TUNEL assay using the In Situ Cell Death Detection Kit, AP (Boehringer Mannheim GmbH, Mannheim, Germany). The slides were counterstained with methyl green.

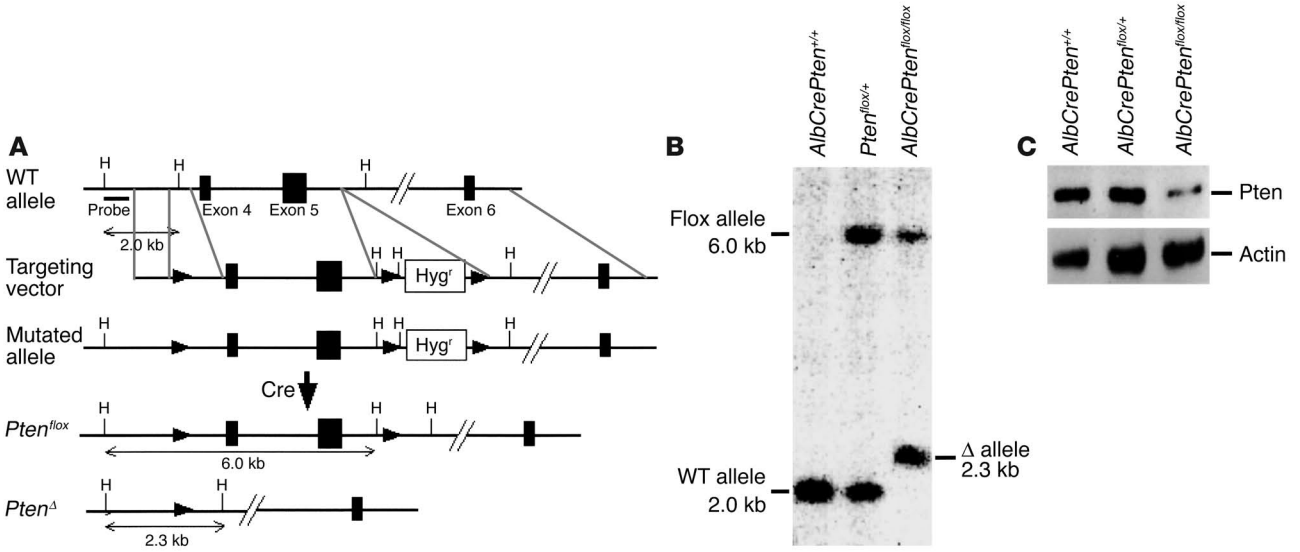

Figure 1
Generation of hepatocyte-specific Pten-deficient (*AlbCrePten*$^{flox/flox}$) mice. (**A**) Targeting strategy. Exons of the murine *Pten* gene are represented by filled boxes, *loxP* sites by filled arrowheads. The probe used to analyze Southern blots is indicated and has been described previously (14). The floxed (*Pten*^{flox}) and deleted (*Pten*$^{\Delta}$) alleles are shown. (**B**) Genomic Southern blot. DNA (20 μg) extracted from total liver cells of the indicated genotypes was digested with *Hin*dIII. The vast majority of total liver cells from *AlbCrePten*$^{flox/flox}$ mice showed deletion of the *Pten* gene. (**C**) Western blot analysis of Pten protein expression by total liver cells of the indicated genotype. Actin, loading control. Liver samples were obtained from 8-week-old mice.

H_2O_2 Production. Liver samples were homogenized (1% w/v) in lysis buffer (0.2 M Tris-HCl, pH 8.0, 0.1 M EDTA, 2% SDS containing 20 mM NaN_3 to inhibit endogenous catalase), and H_2O_2 was assayed using phenol red.

Insulin and glucose tolerance tests and serum insulin measurement. Insulin and glucose tolerance tests were performed on animals that had been starved overnight. Glucose (2 g/kg body weight) or human regular insulin (Eli Lilly and Company, Indianapolis, Indiana, USA) (0.75 U/kg body weight) was administered orally or intraperitoneally, respectively. Blood glucose values at 0, 30, 60, 90, and 120 minutes were measured in tail venous blood using an automated glucose monitor (ARKRAY Inc., Kyoto, Japan). Serum insulin levels following overnight starvation were measured using an ELISA kit according to the manufacturer's protocol (Mercodia, Uppsala, Sweden).

Results

Generation of AlbCrePten$^{flox/flox}$ *mice*. Hepatocyte-specific Pten-deficient mice were generated as described in Figure 1A. *AlbCrePten*$^{flox/flox}$ mice were born alive and appeared healthy. Southern blotting of DNA from

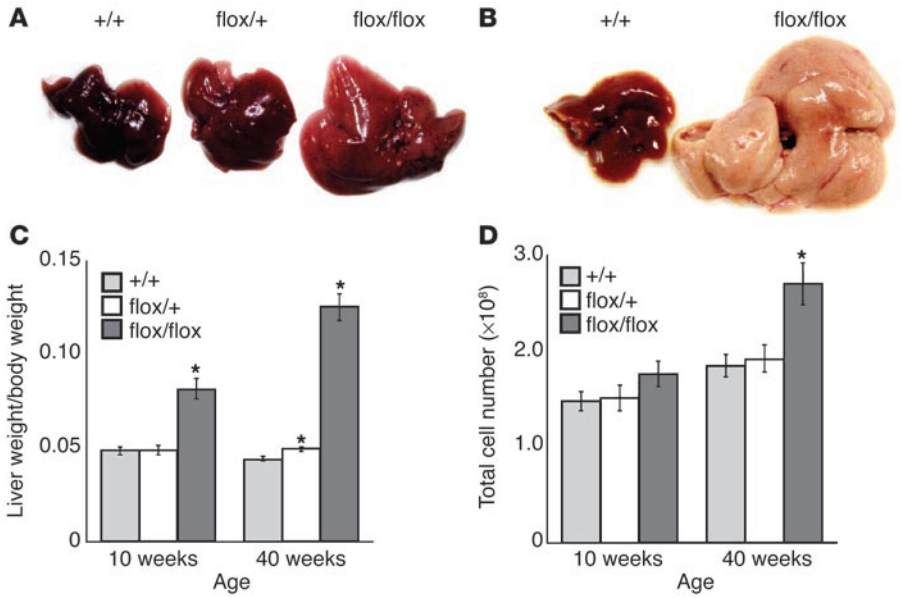

Figure 2
Liver anomalies in *AlbCrePten*$^{flox/flox}$ mice. (**A** and **B**) Macroscopic analyses of livers. Hepatomegaly and pale coloring was observed in 10-week-old (**A**) and 40-week-old (**B**) *AlbCrePten*$^{flox/flox}$ mice. For all panels: +/+, *AlbCrePten*$^{+/+}$; *flox*/+, *AlbCrePten*$^{flox/+}$, and *flox*/*flox*, *AlbCrePten*$^{flox/flox}$ mice. (**C**) Decreased liver weight. The liver weight/body weight ratio was analyzed in +/+, *flox*/+, and *flox*/*flox* mice at 10 weeks (n = 11 mice/group) and 40 weeks (n = 15). For all panels, where appropriate, results are expressed as the mean ± SEM of the indicated number of mice per group. Statistical differences were determined using the Student's t test: $^*P < 0.05$. (**D**) Decreased number of liver cells. Absolute numbers of total liver cells were determined in +/+, *flox*/+, and *flox*/*flox* livers at 10 weeks (n = 7 mice/group) and 40 weeks (n = 7).

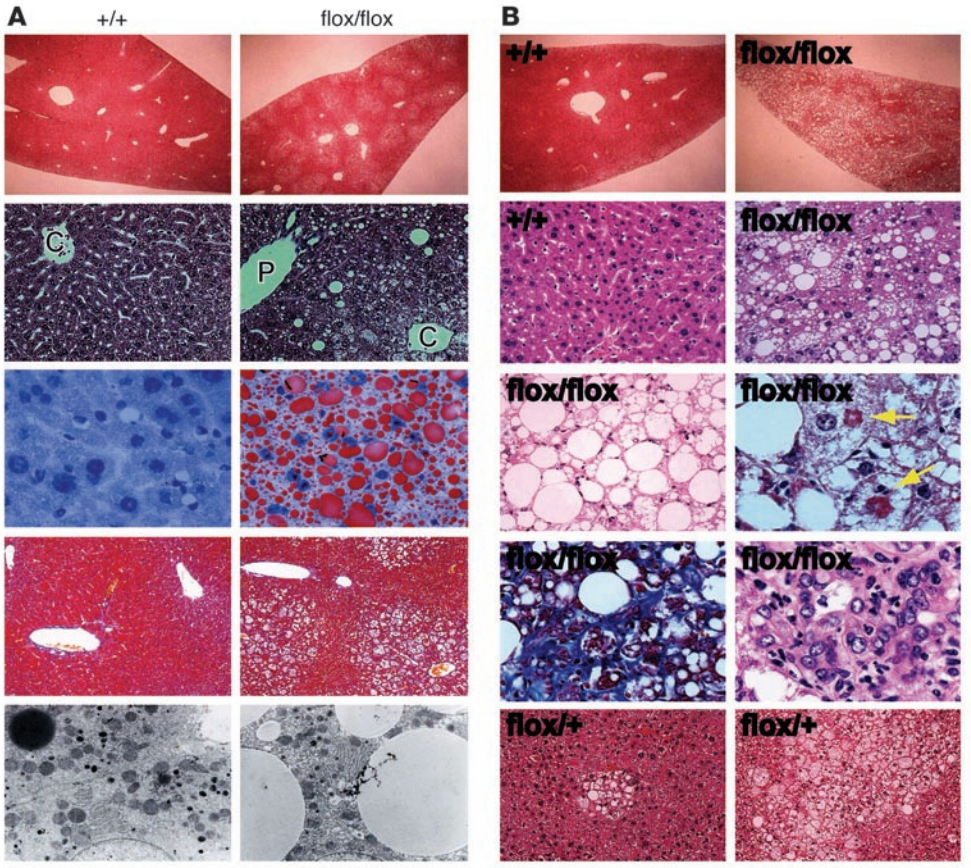

Figure 3
Steatohepatitis in *AlbCrePten*$^{flox/flox}$ mice. (**A**) Histological analyses of liver sections from +/+ and *flox*/*flox* mice sacrificed at 10 weeks of age. The first and second rows show a lower (×10) and higher (×400) magnification of H&E-stained livers, respectively. Lipid accumulation was observed around the central vein area (C), whereas the periportal vein area (P) was almost intact. Lipid accumulation was confirmed by Oil-red O staining (third row). Liver fibrosis was not evident as determined by Azan staining (fourth row). Lipid accumulation was also confirmed by electron microscopy (fifth row). (**B**) Histological analyses of liver sections of +/+, *flox*/+, and *flox*/*flox* mice (without precancerous tumors) sacrificed at 40 weeks of age. The first and second rows show a lower (×10) and higher (×400) magnification of H&E-stained liver sections, respectively. The third row (left) shows an accumulation of lipid in the mutant liver that resembles adipocytes in a fat tissue. Additional features of mutant livers were steatohepatitis and Mallory bodies (third row right, arrows), sinusoidal fibrogenic changes (fourth row left), and an accumulation of inflammatory cells (fourth row right). Focal lipid-laden hepatocytes within diffuse mild fatty changes were noted in the livers of some *flox*/+ mice (fifth row).

total liver cells of 8-week-old mice showed that Cre-mediated recombination of *loxP* sites deleted much of the 6.0-kb *Ptenflox* allele in the majority of cells, leaving the 2.3-kb *Pten*$^{\Delta}$ allele (Figure 1B). Western blotting confirmed a dramatic reduction of Pten protein in livers of 8-week-old mutant mice (Figure 1C). Since hepatocytes compose about 80% of the total liver cell population (23), the *Pten* gene was rendered null in the vast majority of liver cells in *AlbCrePten*$^{flox/flox}$ mice. The faint Pten band visible in the *AlbCrePten*$^{flox/flox}$ liver in Figure 1C is probably due to nonparenchymal liver cells such as bile duct cells, Kupffer cells, lymphocytes, and endothelial cells (23), which do not activate the albumin promoter. Our results are consistent with previous assessments of the efficiency of Cre-*loxP* recombination in total liver cells of *AlbCreTg* mice, observed to be 40% in newborn mice and 75% in 3-week-old mice (15).

Liver anomalies in AlbCrePten$^{flox/flox}$ *mice*. The livers of 10-week-old *AlbCrePten*$^{flox/flox}$ mice were enlarged and light-colored (Figure 2A). At 40 weeks, the livers of *AlbCrePten*$^{flox/flox}$ mice were further enlarged and homogeneously white in color (Figure 2B). The liver weight per body weight ratio of *AlbCrePten*$^{flox/flox}$ mice was increased twofold over that of the WT at 10 weeks, and threefold at 40 weeks (Figure 2C). A more modest but still statistically significant increase in total liver weight was also observed in *AlbCrePten*$^{flox/+}$ mice at 40 weeks. While absolute numbers of *AlbCrePten*$^{flox/flox}$ total liver cells were almost normal at 10 weeks, they had increased significantly (by 1.5-fold) at 40 weeks (Figure 2D).

Steatohepatitis in AlbCrePten$^{flox/flox}$ *mice*. We undertook a closer histological examination of cells in the livers of 10-week-old *AlbCrePten*$^{flox/flox}$ mice. The nuclei of these cells were still centrally located, but the cytoplasm was weakly eosinophilic and contained numerous microvesicular vacuoles. The vacuolar change was observed mainly around the central vein (Figure 3A, first and second rows). Oil Red O staining (Figure 3A, third row) and electron-microscopic examination (Figure 3A, fifth row) revealed that the vacuoles contained lipids. No fibrotic changes (Figure 3A, fourth row), as determined by Azan staining, and no peroxisome proliferation (Supplemental Figure 1) as determined by DAB staining were evident at 10 weeks. Interestingly, steatotic changes were more prominent in male than female mice (data not shown).

Table 1
Biochemical analyses of serum and liver extracts of *AlbCrePten*$^{+/+}$, *AlbCrePten*$^{flox/+}$, and *AlbCrePten*$^{flox/flox}$ mice

	10 weeks old (n = 4)			40 weeks old (n = 4)		
	+/+	flox/+	flox/flox	+/+	flox/+	flox/flox
Serum						
AST (IU/l)	80 ± 8	78 ± 3	95 ± 15	77 ± 7	136 ± 6[A]	337 ± 102[A]
ALT (IU/l)	36 ± 5	39 ± 4	56 ± 10	36 ± 2	55 ± 6[A]	462 ± 167[A]
ALP (IU/l)	233 ± 25	242 ± 37	315 ± 45	191 ± 42	202 ± 46	620 ± 86[A]
Triglyceride (mg/dl)	51 ± 4	45 ± 4	46 ± 1	59 ± 4	60 ± 5	64 ± 3
Total cholesterol (mg/dl)	92 ± 4	92 ± 5	116 ± 11	138 ± 19	115 ± 24	213 ± 47
Liver						
Triglyceride (mg/g)	9.8 ± 0.3	11.4 ± 1.9	87.4 ± 19.8[A]	27.7 ± 8.5	32.3 ± 7.7	215.2 ± 31.1[A]
FFA (μEq/g)	0.41 ± 0.08	0.34 ± 0.04	0.42 ± 0.04	0.41 ± 0.08	0.34 ± 0.04	0.42 ± 0.04
Free cholesterol (mg/g)	0.63 ± 0.01	0.62 ± 0.02	0.62 ± 0.05	0.63 ± 0.01	0.62 ± 0.02	0.62 ± 0.03
Cholesterol esters (mg/g)	0.20 ± 0.09	0.18 ± 0.10	0.44 ± 0.05[A]	0.22 ± 0.10	0.29 ± 0.13	1.46 ± 0.36[A]
Phospholipid (mg/g)	4.7 ± 1.0	5.4 ± 0.2	5.3 ± 0.1	5.1 ± 0.3	4.7 ± 0.1	4.1 ± 0.4
Fatty acid composition						
C16:0 (mg/liver)	47 ± 12		108 ± 20	12 ± 1		131 ± 14[A]
C16:1 (mg/liver)	2 ± 1		10 ± 2[A]	1.4 ± 0.1		21 ± 4[A]
C18:0 (mg/liver)	17 ± 0.4		57 ± 27	3 ± 0.3		13 ± 1[A]
C18:1 (mg/liver)	36 ± 13		163 ± 39[A]	11 ± 0.4		281 ± 19[A]
C18:2 (mg/liver)	63 ± 19		81 ± 12	8 ± 1		23 ± 3[A]

Results are expressed as the mean ± SEM for four mice per group. Statistically significant differences from the WT are shown with an asterisk. Experiments were repeated three times. Statistical differences were determined using the Student's t test: [A]$P < 0.05$.

By 40 weeks, *AlbCrePten*$^{flox/flox}$ livers showed fatty changes of increased severity throughout the hepatic lobule (Figure 3B, first and second rows). The vacuoles had coalesced to form large unilobular vacuoles that displaced the nucleus to the periphery. Indeed, the histological picture of the aged mutant liver resembled that of adipocytes in fat tissues (Figure 3B, third row left). Mallory bodies were frequently observed in the mutant hepatocytes (Figure 3B, third row right). Mild sinusoidal fibrogenic changes (Figure 3B, fourth row left) and accumulations of lobular inflammatory cells (such as lymphocytes and neutrophils) (Figure 3B, fourth row right) were also observed. These histological findings are strikingly similar to those reported for nonalcoholic steatohepatitis (NASH) in humans (24). Focal lipid-laden hepatocytes within diffuse fatty changes were noted in some *AlbCrePten*$^{flox/+}$ livers examined (Figure 3B, fifth row right).

Accumulation of triglyceride and hepatic damage in AlbCrePten$^{flox/flox}$ *mice.* We examined *AlbCrePten*$^{+/+}$, *AlbCrePten*$^{flox/+}$, and *AlbCrePten*$^{flox/flox}$ mice for the status of various biochemical parameters (Table 1). AST, ALT, and ALP levels were not increased in the sera of 10-week-old *AlbCrePten*$^{flox/flox}$ mice but were significantly elevated in 40-week-old mutants. More modest increases in AST and ALT levels were observed in 40-week-old *AlbCrePten*$^{flox/+}$ mice. Thus, steatohepatitis induced in the absence of Pten damages liver function in older mice.

We next evaluated the concentrations of various lipids in samples of liver extracts (Table 1). Triglyceride and cholesterol ester levels were significantly increased in the livers of 10-week-old *AlbCrePten*$^{flox/flox}$ mice, and dramatically elevated in the livers of 40-week-old mutants. However, there were no significant differences in liver concentrations of FFAs, free cholesterol, or phospholipids. Gas chromatographic analysis of total fatty acid composition showed that 16-carbon monounsaturated fatty acids (C16:1) and C18:1 fatty acids were significantly increased in the livers of 10-week-old *AlbCrePten*$^{flox/flox}$ mice. C16:0, C16:1, C18:0, C18:1, and C18:2 fatty acids were also significantly increased in the livers of 40-week-old *AlbCrePten*$^{flox/flox}$ mice, with the greatest increments in C16:1 and C18:1 molecules. Thus, the loss of Pten disrupts several aspects of fat metabolism in the liver.

Expression of adipogenic and lipogenic genes in Pten-deficient hepatocytes. To investigate the triglyceride accumulation in *AlbCrePten*$^{flox/flox}$ livers, we measured the expression of several adipogenic, lipogenic and lipid β-oxidation–related genes in hepatocytes of *AlbCrePten*$^{+/+}$ and *AlbCrePten*$^{flox/flox}$ mice (Figure 4A). RT-PCR analysis revealed a dramatic induction of PPARγ, a key transcriptional activator for adipocyte differentiation (8). Downstream target genes of PPARγ, such as the adipocyte-specific genes adipsin, adiponectin, and aP2, were also induced. Expression levels of PPARα, C/EBPα, C/EBPδ, and other transcriptional activators important for adipocyte differentiation were normal, while expression of C/EBPβ was slightly reduced. Moderate increases were observed in the expression of the PPARα-regulated peroxisomal fatty acid β-oxidation system genes AOX, L-PBE, and PTL. Our data suggest that overexpression of PPARγ induced by an absence of Pten can force upregulation of these PPARα-regulated genes, consistent with previous reports that very high levels of PPARγ can activate transcription of PPARα target genes (10, 12).

Another transcription factor that regulates lipid synthesis is SREBP-1c (25). SREBP-1c expression was moderately elevated in *AlbCrePten*$^{flox/flox}$ livers, as was that of fatty acid–modifying enzymes acting downstream of SREBP-1c such as FAS, ACC, and SCD1. These results indicate that the striking increase in PPARγ observed in the absence of Pten is associated with a moderate increase in expression of SREBP-1c and its target genes.

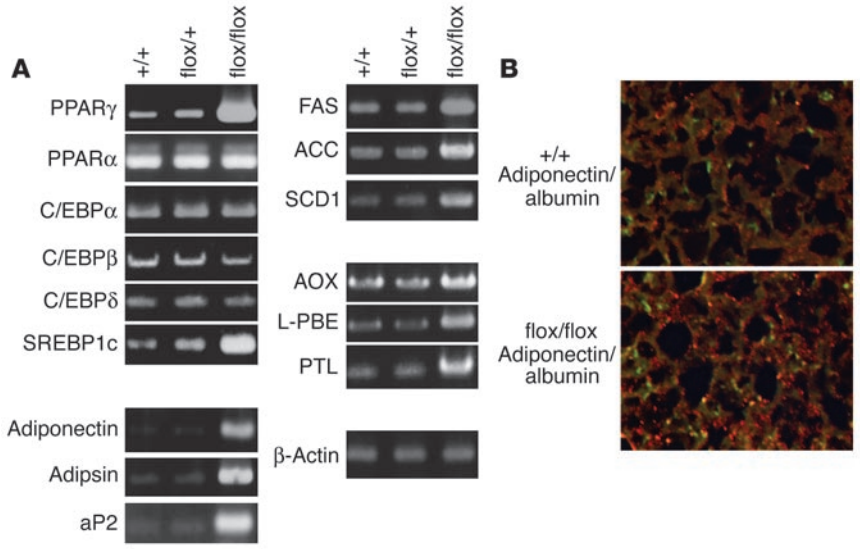

Figure 4
Expression of adipogenic and lipogenic genes in the absence of hepatic Pten. (**A**) RT-PCR analyses of the indicated genes in +/+, *flox*/+, and *flox*/*flox* livers. The relative intensity of each amplified PCR band as measured by NIH Image was as follows: PPARγ +/+, 1; *flox*/+, 2; *flox*/*flox*, 8; PPARα (1, 1, 1); C/EBPα (1, 1, 1); C/EBPβ (1, 1, 0.7); C/EBPδ (1, 1, 1); SREBP1c (1, 1.5, 3); adiponectin (1, 1, 4); adipsin (1, 1, 4); aP2 (1, 1, 4); FAS (1, 1, 3); ACC (1, 1, 2); SCD1 (1, 1, 2); AOX (1, 1, 2); L-PBE (1, 1, 2); PTL (1, 1, 2.5); β-actin (1, 1, 1). Data shown are representative of five independent experiments. (**B**) Expression of adipocyte-specific and hepatocyte-specific markers in the liver. Immunohistochemical double staining using antibodies specific for adiponectin and albumin revealed the strong coexpression of these molecules in *flox*/*flox* liver cells (lower panel) compared with +/+ liver cells (upper panel). Magnification ×1000.

We next performed immunohistochemistry to visualize mutant hepatocytes expressing adiponectin (adipocyte marker) and albumin (hepatocyte marker). Unlike the WT, most *AlbCrePten*$^{flox/flox}$ hepatocytes showed a vivid granular staining pattern with antibody specific to adiponectin (Cy3) (Figure 4B). These adiponectin$^+$ cells also stained positively for albumin (Alexa Fluor 488), confirming that the mutant hepatocytes had acquired expression of an adipocyte-specific marker.

Glucose metabolism in AlbCrePten$^{flox/flox}$ *mice*. The PI3K-PKB/Akt pathway is activated by insulin signaling. To determine if hepatic Pten deficiency affected glucose metabolism, six *AlbCrePten*$^{+/+}$ and six *AlbCrePten*$^{flox/flox}$ mice of 12 weeks of age were starved overnight and subjected to glucose and insulin tolerance tests. *AlbCrePten*$^{flox/flox}$ mice had significantly lower glucose levels than the WT both before and after oral glucose administration (Supplemental Figure 2A). Intraperitoneal insulin injection reduced glucose levels in the mutants by a significantly greater margin compared with the WT even at the 15-minute mark (Supplemental Figure 2B), indicating insulin hypersensitivity. Serum insulin was significantly reduced in *AlbCrePten*$^{flox/flox}$ mice (Supplemental Figure 2C). Thus, Pten deficiency alters both baseline glucose metabolism and insulin sensitivity.

Tumor formation in the livers of AlbCrePten$^{flox/flox}$ *mice*. Pathological examination of 20 *AlbCrePten*$^{+/+}$ and 20 *AlbCrePten*$^{flox/+}$ mice revealed no evidence of hepatic tumors by 40–44 weeks of age. In contrast, macroscopic hepatic tumors were clearly present in 66% (6/9) of male and 30% (3/10) of female *AlbCrePten*$^{flox/flox}$ mice at this age (Figure 5A). Microscopic examination of *AlbCrePten*$^{flox/flox}$ livers revealed nodular lesions resembling liver adenomas that compressed the surrounding nontumorous liver parenchyma (Figure 5B). Cells with large droplets in the cytoplasm were prominent in most adenomas. No such nodular lesions were observed in *AlbCrePten*$^{+/+}$ (data not shown) or *AlbCrePten*$^{flox/+}$ (Figure 5C) livers. Six male and six female *AlbCrePten*$^{flox/flox}$ mice were monitored until sacrifice at age 74–78 weeks. Livers of all these animals showed macroscopic hepatic tumors (Figure 5D). Histological examination revealed that hepatocellular carcinomas (HCCs) were present in five of six male and three of six female *AlbCrePten*$^{flox/flox}$ mice (Figure 5E), while four mutant mice showed benign liver adenomas (data not shown). The HCCs had developed within liver adenomas, and the HCC cells contained many fewer cytoplasmic lipid droplets than the liver adenoma cells. Two *AlbCrePten*$^{flox/flox}$ mice with HCC also showed lung metastases (Figure 5F). These findings indicate that Pten function is essential for preventing liver tumorigenesis.

Tumorigenic anomalies in Pten-deficient hepatocytes. To investigate the molecular basis for the elevated number of hepatocytes and tumor formation in *AlbCrePten*$^{flox/flox}$ mice, hepatocyte proliferation and apoptosis were evaluated by BrdU incorporation and TUNEL assays, respectively. Enhanced BrdU incorporation was observed in 10-week-old *AlbCrePten*$^{flox/+}$ and *AlbCrePten*$^{flox/flox}$ mice (Figure 6A). The percentages of BrdU$^+$ cells in the livers of *AlbCrePten*$^{+/+}$,

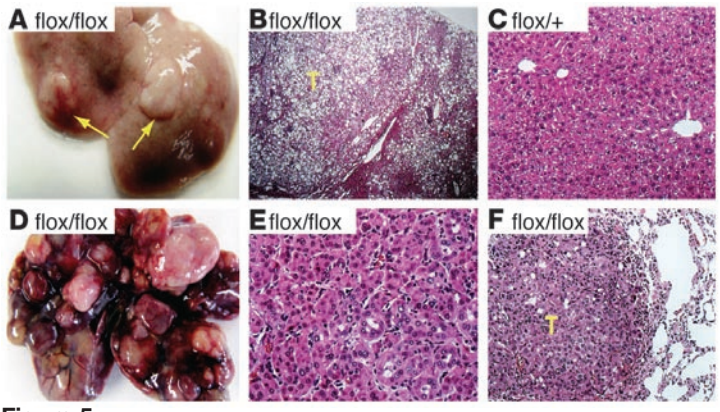

Figure 5
Liver tumors observed in *AlbCrePten*$^{flox/flox}$ mice. (**A**) Macroscopic view of representative liver adenomas (arrows) observed in 9/19 *flox*/*flox* mice of 40–44 weeks of age. (**B**) H&E-stained section of a liver cell adenoma (T) in (**A**) *flox*/*flox* male mouse, showing its distinct demarcation from the surrounding nontumorous liver tissue. The adenoma hepatocytes contain large quantities of lipid. (**C**) H&E-stained section of a *flox*/+ liver (male, 42 weeks). (**D**) Macroscopic view of a representative mutant liver (male) showing the HCCs observed in 8/12 *flox*/*flox* mice at 74–78 weeks of age. (**E**) H&E-stained section of the *flox*/*flox* (male) liver in (**D**), showing an HCC with a trabecular-like arrangement that disrupts normal liver architecture. (**F**) Lung of the mouse in **D**, showing a metastasis (T). Magnifications are ×40 (**B**), ×400 (**C**), ×400 (**E**), and ×400 (**F**).

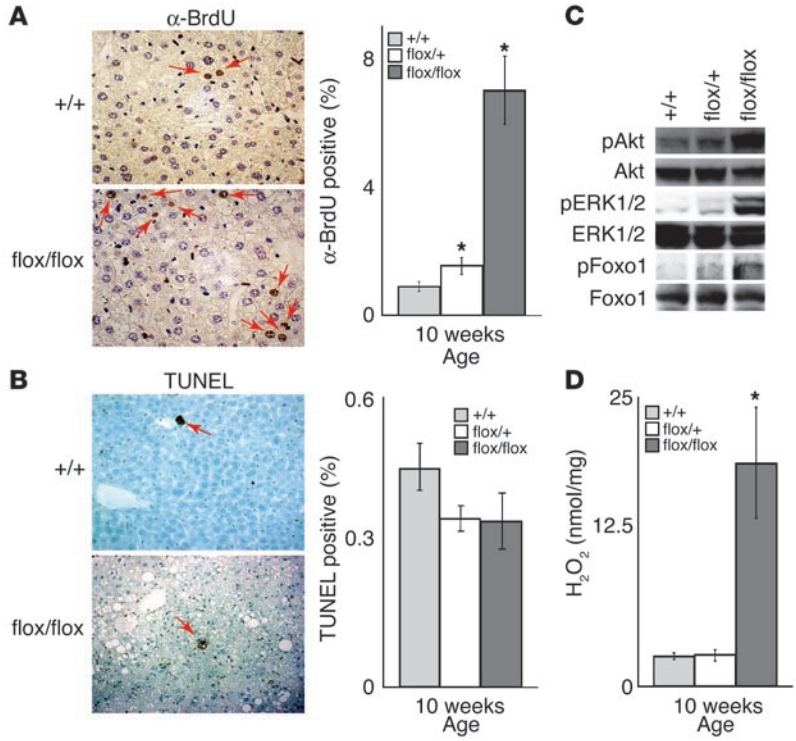

Figure 6
Increased hepatocyte proliferation, phosphorylation of PKB/Akt, Foxo1, and MAPK (ERK1/2), and H_2O_2 production in *AlbCrePten*$^{flox/flox}$ mice. (**A**) Enhanced hepatocyte proliferation. Left panel: BrdU$^+$ hepatocytes (arrows) were counted 4 days after administration of BrdU in drinking water. Right panel: data are expressed as the mean percentage of BrdU$^+$ hepatocytes ± SEM for 1 × 10^4 cells per mouse for four mice per group. (**B**) No effect on apoptosis. Left panel: TUNEL$^+$ hepatocytes (arrows) were counted. Right panel: data are expressed as the mean percentage of TUNEL$^+$ hepatocytes ± SEM for 1 × 10^4 cells per mouse for four mice per group. For **A** and **B**, results shown are one experiment representative of 3 trials. (**C**) Increased phosphorylation of signal transducers. The phosphorylated forms of PKB/Akt, Foxo1, and ERK1/2 in liver lysates of the indicated genotypes were determined by immunoblotting. Total PKB/Akt, Foxo1, and ERK1/2 levels were evaluated as controls. (**D**) Increased H_2O_2 production. H_2O_2 concentrations in liver homogenates from 10-week-old +/+, *flox*/+, and *flox/flox* mice were determined by the phenol red method. Results are expressed as the mean H_2O_2 produced ± SEM for four mice per group and are representative of three trials.

AlbCrePten$^{flox/+}$, and *AlbCrePten*$^{flox/flox}$ mice were 0.9, 1.5, and 7.0%, respectively. No significant differences in hepatocyte apoptosis were observed at either 10 or 40 weeks (Figure 6B).

We previously reported that regulation of PKB/Akt activation by Pten is critical for the normal apoptosis of mouse embryonic fibroblasts and for both proliferation and apoptosis of T cells, B cells, and keratinocytes (14, 18, 26, 27). MAPK, a major signaling molecule acting downstream of Ras, is also activated downstream of PIP3 (28). Our previous demonstration that both MAPK and PKB/Akt are activated in Pten-deficient cells (14, 27) prompted us to analyze the phosphorylation of PKB/Akt and MAPK in hepatocytes from 10-week-old *AlbCrePten*$^{flox/+}$ and *AlbCrePten*$^{flox/flox}$ mice. Indeed, phosphorylated PKB/Akt, its downstream substrate phosphorylated Foxo1, and phosphorylated MAPK (extracellular signal-related kinases 1 and 2; ERK1/2) were significantly increased in *AlbCrePten*$^{flox/flox}$ hepatocytes compared with WT cells (Figure 6B). Thus, hepatocytes require Pten function to regulate PKB/Akt and MAPK signaling.

Increased production of reactive oxygen species (ROS) by hepatocytes has been associated with HCC development (29). We measured levels of H_2O_2 in liver homogenates from 10-week-old *AlbCrePten*$^{flox/+}$ and *AlbCrePten*$^{flox/flox}$ mice. The hepatic H_2O_2 concentration in the mutant liver was increased sevenfold over that of the WT (Figure 6D). Taken together, our data suggest that dysregulation of cell survival signaling pathways and increased production of tumorigenic ROS can combine to drive hepatic tumorigenesis in the absence of Pten.

Discussion

Pten deficiency leads to steatohepatitis. A surprising finding of this study was that Pten deficiency causes lipid accumulation in hepatocytes. As a result, the mutant animals exhibit steatohepatitis similar to that observed in humans with NASH.

Several reports link adipocyte differentiation and the PI3K pathway. Insulin receptor substrate-1–deficient (IRS-1–deficient) pre-adipocyte cell lines stimulated with insulin and WT pre-adipocyte cell lines treated with a PI3K inhibitor both show blocked differentiation, decreased lipid accumulation, and a striking reduction in PPARγ expression (30). *Akt1/Akt2* doubly deficient mice also show impeded adipogenesis due to impaired induction of PPARγ (31). PKB/Akt directly phosphorylates and inactivates Foxo1, and constitutively active Foxo1 inhibits the induction of PPARγ expression and adipocyte differentiation (32). Thus, adipogenesis triggered by the actions of the insulin and IGF-1 receptors and their downstream effectors IRS-1 and IRS-2 requires signaling through the PI3K-PKB/Akt-Foxo1-PPARγ pathway.

Another key player in adipogenesis is SREBP1, a transcription factor that regulates cholesterol and fatty acid homeostasis (25). Insulin-mediated activation of the PI3K-PKB/Akt pathway increases SREBP1c expression in cultured rat hepatocytes (33). Ectopic expression of SREBP1c increases PPARγ expression and activity (34) and enhances FAS expression in cultured fibroblasts and in the livers of transgenic mice (35). SREBP1c promotes adipogenesis in cells stimulated with multiple hormonal inducers (35). Thus, lipid accumulation in Pten-deficient liver may be due to the cooperation of the PI3K-PKB/Akt-Foxo1-PPARγ pathway with PI3K-mediated SREBP1c induction. Indeed, mice that transgenically express PPARγ1 in the liver show massive steatosis (10). Moreover, mice with liver-specific deficiency of PPARγ show the opposite phenotype to our liver-specific Pten-deficient mice — namely, reductions in the lipogenic genes FAS, ACC, and SCD1, decreased hepatic steatosis (in A-ZIP transgenic background), and reduced insulin sensitivity (36, 37). Our data are thus the first to demonstrate that hepatic deficiency of Pten activates lipogenic mechanisms.

Loss of Pten expression in the liver enhances both the expression of the adipocyte-specific markers adiponectin, adipsin,

and aP2, and the appearance of lipid vacuoles in hepatocytes. Immunohistochemistry confirmed that the albumin-expressing cells in mutant livers also expressed adiponectin (Figure 4B). We speculate that the tremendous accumulation of lipids in the mutant hepatocytes was due to an upregulation of PPARγ that resulted in the appearance of adipocyte markers and fat droplets.

Pten deficiency promotes hepatic tumorigenesis. Hepatic deficiency of Pten also leads to the development of liver tumors. Such malignancies can arise due to dysregulation of enzymes that neutralize free radicals. The inducible classical peroxisomal β-oxidation system consists of the H_2O_2-generating enzymes AOX, L-PBE, and PTL (38). Disproportionate increases in these H_2O_2-generating enzymes, coupled with reductions in the H_2O_2-degrading enzymes catalase and glutathione peroxidase, may lead to sustained oxidative stress in the liver (39). As a result, hepatocytes may progressively accumulate lipofuscin, a by-product of ROS-induced lipid peroxidation. The formation of 8-hydroxydeoxyguanosine adducts in liver DNA also occurs under conditions of excess H_2O_2 (40). This metabolically induced oxidative DNA damage may predispose hepatocytes to malignant transformation. Interestingly, hepatocytes with sustained PPARγ activation show increased expression of PPARα-induced H_2O_2-generating enzymes in vitro (12) and in vivo (10). Our data show that Pten deficiency increases the activation of PPARγ- and PPARα-regulated genes, although the expression of PPARα itself is not enhanced. While an increase in endogenous PPARα ligands could theoretically activate PPARα-regulated genes, peroxisome proliferation (which is usually associated with upregulated endogenous PPARα ligands; see ref. 41) was not observed in our Pten-deficient mice. Rather, we theorize that DNA damage due to PPARγ-mediated upregulation of H_2O_2-generating enzymes, coupled with inflammatory cell infiltration plus increased hepatocellular proliferation due to abnormal activation of PKB/Akt and MAPK, may all combine to trigger the hepatic tumorigenesis observed in *AlbCrePten$^{flox/flox}$* mice. Several lines of evidence support our hypothesis. Administration of antioxidants such as ethoxyquin along with peroxisome proliferators retards liver tumorigenesis (42), and peroxisome proliferators capable of inducing HCC development fail to do so in PPARα-null mutant mice (43). Moreover, AOX-deficient mice develop HCC at 10–15 months of age as a result of sustained hyperactivation of PPARα in the liver by its natural ligands (44). These observations bolster our contention that events downstream of PPARα may be critical for HCC onset.

The role of PPARγ in tumorigenesis is controversial. PPARγ activators can promote the development of colon tumors (45, 46), but loss-of-function PPARγ mutations occur in some human colon cancers (47). In mice, PPARγ agonists induce antineoplastic differentiation (48) or growth arrest (49), and suppress chemically induced tumorigenesis (50, 51).

It is unclear whether the altered fatty acid composition observed in the *AlbCrePten$^{flox/flox}$* liver contributes to tumorigenesis. However, increased oleic acid (C18:1) and decreased stearic acid (C18:0) could increase membrane fluidity, leading to the increased metabolism and proliferation (52, 53) characteristic of malignant cells. Analyses of fatty acids present in lipid extracts of transformed cells show a consistent increase in oleic acid content relative to stearic acid (54, 55). Indeed, the ratio of oleic to stearic acid is increased in the livers of mice prone to HCC development, such as hepatitis virus C-core transgenic mice (19). Finally, while stearic acid can inhibit cancer cell growth, oleic acid abrogates this effect (53). The predominance of C18:1 fatty acids in the *AlbCrePten$^{flox/flox}$* liver may induce hepatocytes to divide at an accelerated rate, promoting the acquisition of tumorigenic mutations.

SCD1 expression was also increased in the absence of Pten. SCD1 is involved in the synthesis of oleic and palmitoleic acids (C16:1). SCD1 expression is positively regulated by SREBP1c, C/EBPα, and PPARα (56, 57) but negatively regulated by PPARγ ligands (58). However, PPARγ overexpression in mouse liver enhances SCD1 expression (10), while PPARγ deficiency reduces it (36). Several treatments or conditions that are associated with hepatocarcinogenesis (57, 59) also increase SCD1 expression, and SCD1 levels are higher in rat mammary carcinomas (60) and in mice that are genetically susceptible to hepatocarcinogenesis (61). Sterculic acid, an inhibitor of SCD1 activity, blocks rat mammary carcinogenesis (62). In our study, the increased SREBP1c expression observed in *AlbCrePten$^{flox/flox}$* mice may have induced SCD1 upregulation and an accumulation of monounsaturated fatty acids that may have promoted hepatocarcinogenesis.

Insulin sensitivity in AlbCrePten$^{flox/flox}$ mice. Production of PIP3 by PI3K is necessary for various metabolic responses to insulin, including PKB/Akt activation, glucose transport, and glycogen and lipid synthesis. Because Pten dephosphorylates PIP3, Pten may act as a negative regulator of insulin stimulation. Overexpression of PTEN in 3T3-L1 cells inhibits glucose uptake and GLUT4 translocation in vitro (63), and administration of a Pten antisense oligonucleotide reverses hyperglycemia in *db/db* or *ob/ob* diabetic mice (64). In our study, Pten deficiency in the liver led to insulin hypersensitivity and enhanced glucose clearance. We speculate that Pten deficiency leads to an accumulation of PIP3 that drives constitutive insulin signaling.

Fatty liver is a feature of many mouse models of altered glucose metabolism, including *ob/ob* (65) and aP2-SREBP1c transgenic mice (66). However, in contrast to *AlbCrePten$^{flox/flox}$* mice, these animals show hyperinsulinemia. Increased serum insulin may reduce IRS2 expression, resulting in only weak activation of the PI3K pathway and thus insulin resistance (67). Insulin resistance is a hallmark of human type II diabetes. Our findings thus suggest that molecular strategies that increase PI3K activity, elevate PIP3 concentration, and/or activate PI3K downstream effectors, may constitute novel therapeutic approaches for the treatment of type II diabetes.

Implications of the liver-specific Pten mutation for related human diseases. NASH is a chronic liver disease in humans (68) characterized by steatohepatitis that can progress to irreversible liver cirrhosis and hepatocellular failure. The majority of NASH cases are associated with obesity, diabetes mellitus, and hyperlipidemia, but the underlying mechanism is unknown in the remainder. Whether HCC is a part of the natural history of NASH has been controversial, although some HCC patients do exhibit NASH (68). While hepatic steatosis and insulin hypersensitivity in liver-specific Pten-deficient mice have recently been reported (69), our extended monitoring of our *AlbCrePten$^{flox/flox}$* mice revealed the occurrence of liver tumors and NASH-like pathological features (24) such as steatosis, Mallory bodies, pericellular fibrosis, and the presence of inflammatory cells. PTEN deficiency leading to abnormal PI3K activation may thus underlie some NASH cases. Indeed, hyperleptinemia or estrogen administration can induce NASH in patients, and leptin and estrogen both activate PI3K (70, 71). The fact that our mutant mice go on to develop liver tumors suggests that HCC

is indeed a part of the natural history of NASH. Our results suggest that the controlled blocking of molecules acting downstream of PI3K might provide significant therapeutic benefit to patients predisposed to NASH, liver cirrhosis, or HCC.

Acknowledgments

We thank Tetsuo Noda (Tohoku University), Nobuya Inagaki, Nobuhiro Ban, Manabu Hashimoto, Chihoko Horie, Miyuki Natsui, Takako Sasaki, and Miki Satoh (all of Akita University) for helpful discussions and technical assistance. This work was supported by grants from the Ministry of Education, Science, Sports and Culture, Japan; the AstraZeneca Research Foundation; the Ono Medical Research Foundation; the Naito Foundation; the Sumitomo Foundation; the Foundation for Promotion of Cancer Research; the Japanese Medical Association; the Sagawa Cancer Research Promotion Foundation; and the Princess Takamatsu Cancer Research Fund (02-23403).

Received for publication November 11, 2003, and accepted in revised form April 27, 2004.

Address correspondence to: Akira Suzuki, Department of Molecular Biology, Akita University, School of Medicine, Hondo 1-1-1, Akita, Akita 010-8543, Japan. Phone: 81-18-884-6077; Fax: 81-18-884-6077; E-mail: suzuki@med.akita-u.ac.jp.

Yasuo Horie and Akira Suzuki are co-senior authors.

Sumio Watanabe, Tak Wah Mak, and Toru Nakano contributed equally to this work.

1. Li, J., et al. 1997. PTEN, a putative protein tyrosine phosphatase gene mutated in human brain, breast, and prostate cancer. *Science.* **275**:1943–1947.
2. Myers, M.P., et al. 1998. The lipid phosphatase activity of PTEN is critical for its tumor suppressor function. *Proc. Natl. Acad. Sci. U. S. A.* **95**:13513–13518.
3. Maehama, T., and Dixon, J.E. 1998. The tumor suppressor, PTEN/MMAC1, dephosphorylates the lipid second messenger, phosphatidylinositol 3,4,5-trisphosphate. *J. Biol. Chem.* **273**:13375–13378.
4. Yao, Y.J., et al. 1999. PTEN/MMAC1 mutations in hepatocellular carcinomas. *Oncogene.* **18**:3181–3185.
5. Hu, T.H., et al. 2003. Expression and prognostic role of tumor suppressor gene PTEN/MMAC1/TEP1 in hepatocellular carcinoma. *Cancer.* **97**:1929–1940.
6. Okano, J., et al. 2003. Hepatocyte growth factor exerts a proliferative effect on oval cells through the PI3K/AKT signaling pathway. *Biochem. Biophys. Res. Commun.* **309**:298–304.
7. Suzuki, A., et al. 2000. Hepatocyte growth factor promotes cell survival from fas-mediated cell death in hepatocellular carcinoma cells via Akt activation and Fas-death-inducing signaling complex suppression. *Hepatology.* **32**:796–802.
8. Tontonoz, P., Hu, E., Graves, R.A., Budavari, A.I., and Spiegelman, B.M. 1994. mPPAR gamma 2: tissue-specific regulator of an adipocyte enhancer. *Genes Dev.* **8**:1224–1234.
9. Tontonoz, P., Hu, E., and Spiegelman, B.M. 1994. Stimulation of adipogenesis in fibroblasts by PPAR gamma 2, a lipid-activated transcription factor. *Cell.* **79**:1147–1156.
10. Yu, S., et al. 2003. Adipocyte-specific gene expression and adipogenic steatosis in the mouse liver due to peroxisome proliferator-activated receptor gamma1 (PPARgamma1) overexpression. *J. Biol. Chem.* **278**:498–505.
11. Surapureddi, S., et al. 2002. Identification of a transcriptionally active peroxisome proliferator-activated receptor alpha-interacting cofactor complex in rat liver and characterization of PRIC285 as a coactivator. *Proc. Natl. Acad. Sci. U. S. A.* **99**:11836–11841.
12. Marcus, S.L., et al. 1993. Diverse peroxisome proliferator-activated receptors bind to the peroxisome proliferator-responsive elements of the rat hydratase/dehydrogenase and fatty acyl-CoA oxidase genes but differentially induce expression. *Proc. Natl. Acad. Sci. U. S. A.* **90**:5723–5727.
13. Kishimoto, H., et al. 2003. Physiological functions of Pten in mouse tissues. *Cell Struct. Funct.* **28**:11–21.
14. Suzuki, A., et al. 2001. T cell-specific loss of Pten leads to defects in central and peripheral tolerance. *Immunity.* **14**:523–534.
15. Postic, C., and Magnuson, M.A. 2000. DNA excision in liver by an albumin-Cre transgene occurs progressively with age. *Genesis.* **26**:149–150.
16. Suzuki, A., et al. 1998. High cancer susceptibility and embryonic lethality associated with mutation of the PTEN tumor suppressor gene in mice. *Curr. Biol.* **8**:1169–1178.
17. Moldeus, P., Hogberg, J., and Orrenius, S. 1978. Isolation and use of liver cells. *Methods Enzymol.* **52**:60–71.
18. Stambolic, V., et al. 1998. Negative regulation of PKB/Akt-dependent cell survival by the tumor suppressor PTEN. *Cell.* **95**:29–39.
19. Moriya, K., et al. 2001. Increase in the concentration of carbon 18 monounsaturated fatty acids in the liver with hepatitis C: analysis in transgenic mice and humans. *Biochem. Biophys. Res. Commun.* **281**:1207–1212.
20. Todoroki, T., Imai, K., Matsumoto, K., and Kato, S. 1983. Initial deactivation of florisil adsorbent for column chromatographic separation. *Analyst.* **108**:1267–1269.
21. Morrison, W.R., and Smith, L.M. 1964. Preparation of fatty acid methyl esters and dimethylacetals from lipids with boron fluoride-methanol. *J. Lipid Res.* **5**:600–608.
22. Bondia, E.M., Castellote, A.I., Lopez, M.C., and Rivero, M. 1994. Determination of plasma fatty acid composition in neonates by gas chromatography. *J. Chromatogr. B. Biomed. Appl.* **658**:369–374.
23. Jones, A.L., and Spring-Mills, E. 1983. The liver and gallbladder. In *Histology: cell and tissue biology.* 5th edition. L. Weiss, editor. Macmillan Press. London, United Kingdom. 707–748.
24. Matteoni, C.A., et al. 1999. Nonalcoholic fatty liver disease: a spectrum of clinical and pathological severity. *Gastroenterology.* **116**:1413–1419.
25. Tontonoz, P., Kim, J.B., Graves, R.A., and Spiegelman, B.M. 1993. ADD1: a novel helix-loop-helix transcription factor associated with adipocyte determination and differentiation. *Mol. Cell. Biol.* **13**:4753–4759.
26. Suzuki, A., et al. 2003. Critical roles of Pten in B cell homeostasis and immunoglobulin class switch recombination. *J. Exp. Med.* **197**:657–667.
27. Suzuki, A., et al. 2003. Keratinocyte-specific Pten deficiency results in epidermal hyperplasia, accelerated hair follicle morphogenesis and tumor formation. *Cancer Res.* **63**:674–681.
28. Shan, X., et al. 2000. Deficiency of PTEN in Jurkat T cells causes constitutive localization of Itk to the plasma membrane and hyperresponsiveness to CD3 stimulation. *Mol. Cell. Biol.* **20**:6945–6957.
29. Cerutti, P.A. 1994. Oxy-radicals and cancer. *Lancet.* **344**:862–863.
30. Fasshauer, M., et al. 2001. Essential role of insulin receptor substrate 1 in differentiation of brown adipocytes. *Mol. Cell. Biol.* **21**:319–329.
31. Peng, X.D., et al. 2003. Dwarfism, impaired skin development, skeletal muscle atrophy, delayed bone development, and impeded adipogenesis in mice lacking Akt1 and Akt2. *Genes Dev.* **17**:1352–1365.
32. Nakae, J., et al. 2003. The forkhead transcription factor Foxo1 regulates adipocyte differentiation. *Dev. Cell.* **4**:119–129.
33. Fleischmann, M., and Iynedjian, P.B. 2000. Regulation of sterol regulatory-element binding protein 1 gene expression in liver: role of insulin and protein kinase B/cAkt. *Biochem. J.* **349**:13–17.
34. Kim, J.B., Wright, H.M., Wright, M., and Spiegelman, B.M. 1998. ADD1/SREBP1 activates PPARgamma through the production of endogenous ligand. *Proc. Natl. Acad. Sci. U. S. A.* **95**:4333–4337.
35. Kim, J.B., and Spiegelman, B.M. 1996. ADD1/SREBP1 promotes adipocyte differentiation and gene expression linked to fatty acid metabolism. *Genes Dev.* **10**:1096–1107.
36. Matsusue, K., et al. 2003. Liver-specific disruption of PPARgamma in leptin-deficient mice improves fatty liver but aggravates diabetic phenotypes. *J. Clin. Invest.* **111**:737–747. doi:10.1172/JCI200317223.
37. Gavrilova, O., et al. 2003. Liver peroxisome proliferator-activated receptor gamma contributes to hepatic steatosis, triglyceride clearance, and regulation of body fat mass. *J. Biol. Chem.* **278**:34268–34276.
38. Reddy, J.K., and Hashimoto, T. 2001. Peroxisomal beta-oxidation and peroxisome proliferator-activated receptor alpha: an adaptive metabolic system. *Annu. Rev. Nutr.* **21**:193–230.
39. Gonzalez, F.J., Peters, J.M., and Cattley, R.C. 1998. Mechanism of action of the nongenotoxic peroxisome proliferators: role of the peroxisome proliferator-activator receptor alpha. *J. Natl. Cancer Inst.* **90**:1702–1709.
40. Kasai, H., Okada, Y., Nishimura, S., Rao, M.S., and Reddy, J.K. 1989. Formation of 8-hydroxydeoxyguanosine in liver DNA of rats following long-term exposure to a peroxisome proliferator. *Cancer Res.* **49**:2603–2605.
41. Ringeissen, S., et al. 2003. Potential urinary and plasma biomarkers of peroxisome proliferation in the rat: identification of N-methylnicotinamide and N-methyl-4-pyridone-3-carboxamide by ^{1}H nuclear magnetic resonance and high performance liquid chromatography. *Biomarkers.* **8**:240–271.
42. Rao, M.S., Lalwani, N.D., Watanabe, T.K., and Reddy, J.K. 1984. Inhibitory effect of antioxidants ethoxyquin and 2(3)-*tert*-butyl-4-hydroxyanisole on hepatic tumorigenesis in rats fed ciprofibrate, a peroxisome proliferator. *Cancer Res.* **44**:1072–1076.
43. Peters, J.M., Cattley, R.C., and Gonzalez, F.J. 1997. Role of PPARalpha in the mechanism of action of the nongenotoxic carcinogen and peroxisome proliferator Wy-14,643. *Carcinogenesis.* **18**:2029–2033.
44. Fan, C.Y., et al. 1998. Steatohepatitis, spontaneous peroxisome proliferation and liver tumors in

mice lacking peroxisomal fatty acyl-CoA oxidase. Implications for peroxisome proliferator-activated receptor alpha natural ligand metabolism. *J. Biol. Chem.* **273**:15639–15645.
45. Lefebvre, A.M., et al. 1998. Activation of the peroxisome proliferator-activated receptor gamma promotes the development of colon tumors in C57BL/6J-APC$^{Min/+}$ mice. *Nat. Med.* **4**:1053–1057.
46. Saez, E., et al. 1998. Activators of the nuclear receptor PPARgamma enhance colon polyp formation. *Nat. Med.* **4**:1058–1061.
47. Sarraf, P., et al. 1999. Loss-of-function mutations in PPAR gamma associated with human colon cancer. *Mol. Cell.* **3**:799–804.
48. Demetri, G.D., et al. 1999. Induction of solid tumor differentiation by the peroxisome proliferator-activated receptor-gamma ligand troglitazone in patients with liposarcoma. *Proc. Natl. Acad. Sci. U. S. A.* **96**:3951–3956.
49. Kitamura, S., et al. 1999. Peroxisome proliferator-activated receptor gamma induces growth arrest and differentiation markers of human colon cancer cells. *Jpn. J. Cancer Res.* **90**:75–80.
50. Osawa, E., et al. 2003. Peroxisome proliferator-activated receptor gamma ligands suppress colon carcinogenesis induced by azoxymethane in mice. *Gastroenterology.* **124**:361–367.
51. Girnun, G.D., et al. 2002. APC-dependent suppression of colon carcinogenesis by PPARgamma. *Proc. Natl. Acad. Sci. U. S. A.* **99**:13771–13776.
52. Habib, N.A., et al. 1987. Stearic acid and carcinogenesis. *Br. J. Cancer.* **56**:455–458.
53. Fermor, B.F., et al. 1992. Fatty acid composition of normal and malignant cells and cytotoxicity of stearic, oleic and sterculic acids in vitro. *Eur. J. Cancer.* **28A**:1143–1147.
54. Apostolov, K., Barker, W., Catovsky, D., Goldman, J., and Matutes, E. 1985. Reduction in the stearic to oleic acid ratio in leukaemic cells—a possible chemical marker of malignancy. *Blut.* **50**:349–354.
55. Wood, C.B., et al. 1985. Reduction in the stearic to oleic acid ratio in human malignant liver neoplasms. *Eur. J. Surg. Oncol.* **11**:347–348.
56. Bene, H., Lasky, D., and Ntambi, J.M. 2001. Cloning and characterization of the human stearoyl-CoA desaturase gene promoter: transcriptional activation by sterol regulatory element binding protein and repression by polyunsaturated fatty acids and cholesterol. *Biochem. Biophys. Res. Commun.* **284**:1194–1198.
57. Miller, C.W., and Ntambi, J.M. 1996. Peroxisome proliferators induce mouse liver stearoyl-CoA desaturase 1 gene expression. *Proc. Natl. Acad. Sci. U. S. A.* **93**:9443–9448.
58. Kurebayashi, S., Hirose, T., Miyashita, Y., Kasayama, S., and Kishimoto, T. 1997. Thiazolidinediones downregulate stearoyl-CoA desaturase 1 gene expression in 3T3-L1 adipocytes. *Diabetes.* **46**:2115–2118.
59. Thai, S.F., Allen, J.W., DeAngelo, A.B., George, M.H., and Fuscoe, J.C. 2001. Detection of early gene expression changes by differential display in the livers of mice exposed to dichloroacetic acid. *Carcinogenesis.* **22**:1317–1322.
60. Lu, J., Pei, H., Kaeck, M., and Thompson, H.J. 1997. Gene expression changes associated with chemically induced rat mammary carcinogenesis. *Mol. Carcinog.* **20**:204–215.
61. Falvella, F.S., et al. 2002. Stearoyl-CoA desaturase 1 (Scd1) gene overexpression is associated with genetic predisposition to hepatocarcinogenesis in mice and rats. *Carcinogenesis.* **23**:1933–1936.
62. Khoo, D.E., et al. 1991. Manipulation of body fat composition with sterculic acid can inhibit mammary carcinomas in vivo. *Br. J. Cancer.* **63**:97–101.
63. Nakashima, N., Sharma, P.M., Imamura, T., Bookstein, R., and Olefsky, J.M. 2000. The tumor suppressor PTEN negatively regulates insulin signaling in 3T3-L1 adipocytes. *J. Biol. Chem.* **275**:12889–12895.
64. Butler, M., et al. 2002. Specific inhibition of PTEN expression reverses hyperglycemia in diabetic mice. *Diabetes.* **51**:1028–1034.
65. Zhang, Y., et al. 1994. Positional cloning of the mouse obese gene and its human homologue. *Nature.* **372**:425–432.
66. Shimomura, I., et al. 1998. Insulin resistance and diabetes mellitus in transgenic mice expressing nuclear SREBP-1c in adipose tissue: model for congenital generalized lipodystrophy. *Genes Dev.* **12**:3182–3194.
67. Shimomura, I., et al. 2000. Decreased IRS-2 and increased SREBP-1c lead to mixed insulin resistance and sensitivity in livers of lipodystrophic and ob/ob mice. *Mol. Cell.* **6**:77–86.
68. Younossi, Z.M., et al. 1998. Nonalcoholic fatty liver disease: assessment of variability in pathologic interpretations. *Mod. Pathol.* **11**:560–565.
69. Stiles, B., et al. 2004. Liver-specific deletion of negative regulator Pten results in fatty liver and insulin hypersensitivity. *Proc. Natl. Acad. Sci. U. S. A.* **101**:2082–2087.
70. Zhao, A.Z., Huan, J.N., Gupta, S., Pal, R., and Sahu, A. 2002. A phosphatidylinositol 3-kinase phosphodiesterase 3B-cyclic AMP pathway in hypothalamic action of leptin on feeding. *Nat. Neurosci.* **5**:727–728.
71. Simoncini, T., et al. 2000. Interaction of oestrogen receptor with the regulatory subunit of phosphatidylinositol-3-OH kinase. *Nature.* **407**:538–541.